A Theory of Three-Dimensional Parachute Dynamic Stability

FRANK M. WHITE* AND DEAN F. WOLF†
University of Rhode Island, Kingston, R. I.

The three-dimensional motion of a freely descending parachute is studied with a five-degree-of-freedom analysis (the roll motion is neglected). The equations of motion are nondimensionalized and the resulting parameters discussed. Exact expressions are given for the longitudinal and lateral small-disturbance stability of the familiar gliding motion of parachutes. The breakdown of these small-disturbance expressions is illustrated by exact large-disturbance studies. A large longitudinal disturbance of most parachutes will result in a large pitching motion, whereas a large lateral (out of the glide plane) disturbance will usually cause a large angle vertical coning motion. Exact algebraic expressions are given for the coning mode, which is a stable rotation, and a small amount of available coning data is included for comparison. Some parametric computer studies of the various motions are also shown.

Nomenclature

A	=	canopy nominal area
B_m, B_i	=	dimensionless canopy inertia, see Eqs. (25) and (26)
C_N, C_T	=	canopy normal and tangent force coefficients, Eq. (7)
$C_{N\alpha}$, $C_{T\alpha}$	=	force coefficient slopes at the glide point, Fig. 2
D_0	=	canopy nominal diam
E_i, C_i, K_i	=	consts in the small-disturbance analysis
g	=	acceleration of gravity
I, i	=	system moment of inertia, Eq. (6)
L	=	length between canopy and load centroids, Fig. 1
m, k	=	system mass, Eq. (6)
M, N	=	aerodynamic moment components
P, p, Q, q	=	angular velocity components, Fig. 1 and Eq. (4)
r	=	dimensionless mass ratio, Eq. (6)
t, t^*	=	time, Eq. (4)
T	=	period of oscillation
U, u, V, v, W, w	=	velocity components, Fig. 1 and Eq. (4)
x, y, z	=	Cartesian coordinates
X, Y, Z	=	aerodynamic force components
α	=	canopy angle of attack
β, γ	=	coning angles, Fig. 10
λ	=	characteristic root in small-disturbance theory
ψ, θ, ϕ	=	Euler angles between earth and body axes
ρ	=	fluid density

Subscripts

c	=	canopy
ch	=	canopy hydrodynamic
1	=	earth axes
0	=	at the glide point $\alpha = \alpha_0$
p	=	payload

Superscripts

$(\ )^*$	=	dimensionless quantity
$(\ )'$	=	small-disturbance variable
$(\dot{\ })$	=	derivative with respect to t*

Presented at the 1966 AIAA Aerodynamic Deceleration Systems Conference, Houston, Texas, September 7–9, 1966 (no paper number; published in a bound volume of meeting papers); submitted November 29, 1966; revision received June 19, 1967. The work reported here was supported by Division 9324 of the Sandia Corporation, Albuquerque, N. Mex., for the U.S. Atomic Energy Commission.

* Professor of Mechanical Engineering and Applied Mechanics. Associate Fellow AIAA.

† Graduate Fellow, Department of Mechanical Engineering and Applied Mechanics. Associate Member AIAA.

Introduction

THE parachute is a well-known method of achieving aerodynamic retardation, and many different types of parachutes have been designed and tested.[1] Some of the engineering properties are now available, such as the static aerodynamic coefficients[2] and opening shock and strength data.[3] However, the reasons for the various dynamic instabilities of a parachute have not yet been fully explained. One problem is that dynamic stability testing of parachutes is difficult, and usually gives crude results.[4] Also, to theorize on parachute instability requires a nonlinear three-dimensional analysis with several assumptions that are difficult to justify.

The general motion of a parachute can be separated into four effects: 1) steady vertical descent, 2) steady gliding, 3) large angle pitching oscillation, and 4) large angle coning motion. The first type of motion, vertical descent, was analyzed by linear theory in early work by Henn[5] and Brown.[6] These papers contained certain errors in their equations of motion, as discussed by Lester,[7] who gave a careful derivation of the equations but did not attempt any solutions. A recent study by Heinrich and Rust[8] gives a conservative criterion for linearized dynamic stability of vertical plane motion.

The second motion, steady gliding, has been discussed under static conditions by Heinrich.[9] The present paper apparently gives the first criterion for longitudinal and lateral dynamic stability of a steady gliding motion.

The third motion, pitching oscillation, has been analyzed in computer solutions by Ludwig and Heins,[10–12] with application to personnel guide surface parachutes. No general criteria were given by these authors for stability.

The final motion, coning, has been noted in tests,[9,13] but the present paper is apparently the first to analyze coning theoretically.

Equations of Motion

Simplifying Assumptions

To reduce the problem to one which will yield numerical results, the following assumptions have been made:

1) The system consists of a symmetric parachute rigidly connected to a neutral payload.

2) The aerodynamic force and hydrodynamic inertia of the payload are negligible.

3) There are five degrees of freedom, with the roll of the parachute about its axis of symmetry being ignored.

4) The hydrodynamic mass and moment of inertia tensors of the canopy are approximated by single scalar values.

5) The aerodynamic forces are assumed quasistatic as based on the instantaneous angle of attack of the canopy.

6) The canopy center of pressure is taken at the canopy centroid. Apparently, the actual center of pressure of a parachute canopy has not been tested.

7) A flat earth is assumed with no winds.

These assumptions, although restrictive, still allow one to obtain considerable information about parachute stability.

Equations of Motion

The equations of motion use the previous assumptions to simplify the general derivation given in Chap. 4 of the text by Etkin.[14] It is convenient to use body axes (x, y, z) for the stability analysis and earth-fixed axes (x_1, y_1, z_1) to compute the trajectory. These two right-handed systems are illustrated in Fig. 1. In the body axis system, there are linear velocities (U, V, W), angular velocities (P, Q), aerodynamic forces (X, Y, Z), and aerodynamic moments (M, N). The z axis is the axis of symmetry of the parachute. The earth-fixed axes are aligned with the body axes by a series of three Euler angle rotations in the following order:

ψ = a rotation about z_1

θ = a rotation about y_2 (position of y_1 after ψ)

ϕ = a rotation about x_3 (position of x_1 after ψ and θ)

The five force and moment equations in the body axis system then become

$$\begin{aligned} m(dU/dt + QW) &= X - (m_p + m_c)g\sin\theta \\ m(dV/dt - PW) &= Y + (m_p + m_c)g\cos\theta\sin\phi \\ m(dW/dt + PV - QU) &= Z + (m_p + m_c)g\cos\theta\cos\phi \\ I(dP/dt) &= M - m_p g L_p\cos\theta\sin\phi + m_c g L_c\cos\theta\sin\phi \\ I(dQ/dt) &= N + \sin\theta(m_c g L_c - m_p g L_p) \end{aligned} \tag{1}$$

where $m = (m_c + m_p + m_{ch})$ and the moment of inertia $I = (I_c + I_p + I_{ch})$ include the hydrodynamic or apparent inertia of the canopy. The angular velocities are related to the Euler angles by the expressions

$$d\theta/dt = Q\cos\phi \qquad d\phi/dt = P + Q\sin\phi\tan\theta \tag{2}$$

Equations (1) and (2) are seven equations in the seven unknowns (U, V, W, P, Q, θ, ϕ). The lengths L_c and L_p relate the centroids of the canopy and payload to the system centroid, as shown in Fig. 1. Since the canopy is assumed to provide all the aerodynamic forces and moments, the angle of attack is taken to be the instantaneous angle α between the velocity V_c of the canopy centroid and the axis of symmetry z. This angle α is also shown in Fig. 1.

If desired, the system trajectory in earth-fixed coordinates can be calculated from the following relations:

$$\begin{aligned} d\psi/dt &= Q\sin\phi\sec\theta \\ dx_1/dt &= U\cos\theta\cos\psi + V(\sin\phi\sin\theta\cos\psi - \cos\phi\sin\psi) + W(\cos\phi\sin\theta\cos\psi + \sin\phi\sin\psi) \\ dy_1/dt &= U\cos\theta\sin\psi + V(\sin\phi\sin\theta\sin\psi + \cos\phi\cos\psi) + W(\cos\phi\sin\theta\sin\psi - \sin\phi\cos\psi) \\ dz_1/dt &= -U\sin\theta + V\sin\phi\cos\theta + W\cos\phi\cos\theta \end{aligned} \tag{3}$$

However, only Eqs. (1) and (2) are needed for a stability study.

Nondimensional Equations

It is convenient to define dimensionless variables based upon the system length L and the steady glide speed V_0, as follows:

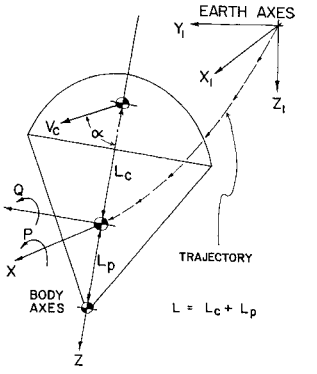

Fig. 1 Sketch of system geometry and coordinate systems.

$$u = \frac{U}{V_0} \qquad v = \frac{V}{V_0} \qquad w = \frac{W}{V_0}$$
$$p = \frac{LP}{V_0} \qquad q = \frac{LQ}{V_0} \qquad t^* = \frac{V_0 t}{L} \tag{4}$$

Substitution into Eqs. (1) gives the following dimensionless equations of motion, whose analysis constitutes the remainder of this paper.

$$\begin{aligned} \frac{du}{dt^*} &= -\frac{C_N V_c^{*2}\left(u - \dfrac{q}{1+r_c}\right)}{2k(V_c^{*2} - w^2)^{1/2}} - \frac{C_{T_0}}{2k}\sin\theta - qw \\ \frac{dv}{dt^*} &= -\frac{C_N V_c^{*2}\left(v + \dfrac{p}{1+r_c}\right)}{2k(V_c^{*2} - w^2)^{1/2}} + \frac{C_{T_0}}{2k}\cos\theta\sin\phi + pw \\ \frac{dw}{dt^*} &= -\frac{C_T V_c^{*2}}{2k} + \frac{C_{T_0}}{2k}\cos\theta\cos\phi - pv + qu \\ \frac{dp}{dt^*} &= -\frac{C_N V_c^{*2}\left(v + \dfrac{p}{1+r_c}\right)}{2i(1+r_c)(V_c^{*2} - w^2)^{1/2}} - \frac{C_{T_0} r_{ch}}{2i(1+r_c)}\cos\theta\sin\phi \\ \frac{dq}{dt^*} &= \frac{C_N V_c^{*2}\left(u - \dfrac{q}{1+r_c}\right)}{2i(1+r_c)(V_c^{*2} - w^2)^{1/2}} - \frac{C_{T_0} r_{ch}}{2i(1+r_c)}\sin\theta \end{aligned} \tag{5}$$

The dimensionless parameters in Eqs. (5) are defined as

$$\begin{aligned} r_c &= (m_c + m_{ch})/m_p \qquad r_{ch} = m_{ch}/(m_c + m_p) \\ k &= m/\rho AL \qquad i = I/\rho AL^3 \\ C_{T0} &= (m_c + m_p)g/\tfrac{1}{2}\rho V_0^2 A \end{aligned} \tag{6}$$

where ρ is the fluid density and A is a reference area, usually the nominal cloth area of the parachute. The quantities C_N and C_T are the normal and tangential aerodynamic force coefficients of the canopy,

$$C_N = (X^2 + Y^2)^{1/2}/\tfrac{1}{2}\rho V_c^2 A \qquad C_T = -Z/\tfrac{1}{2}\rho V_c^2 A \tag{7}$$

which, from assumption 5, are taken to depend quasi-statically upon the instantaneous angle-of-attack α of the canopy (Fig. 1),

$$\alpha = \arctan\{1/w[(u - q/1 + r_c)^2 + (v + p/1 + r_c)^2]^{1/2}\} \tag{8}$$

Finally, the quantity V_c^* is the dimensionless canopy velocity,

$$V_c^{*2} = w^2 + [u - (q/1 + r_c)]^2 + [v + (p/1 + r_c)]^2 \tag{9}$$

Equations (2) and (3) will not be rewritten because their

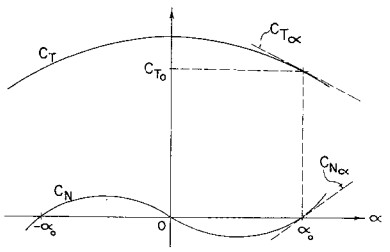

Fig. 2 Typical force coefficient curves for a parachute, showing the linear slope approximation.

dimensionless form is exactly equivalent. These equations are nonlinear but may easily be solved for particular cases on a digital computer. Before discussing any computer solutions, let us derive a small disturbance stability criterion.

Glide-Point Small-Disturbance Analysis

Because of the unusual shape of the force coefficient curves, most parachutes do not fall vertically, even if they are stable. Figure 2 is a sketch of typical canopy coefficients as a function of the angle of attack. The C_N curve is antisymmetric, because the normal force changes direction, acting away from the centerline if α is between $-\alpha_0$ and $+\alpha_0$. A parachute cannot remain at the point ($\alpha = 0$), even though the normal force is zero there, because any slight disturbance will drive the chute away from the origin because of the induced outward normal force. This condition is termed static instability and is derived rigorously in this section. However, as discussed by Heinrich,[9] the point ($\alpha = \alpha_0$) is statically stable, since a slight disturbance causes a normal force which returns the chute back toward α_0. Heinrich calls α_0 the "stable glide point," because the chute will glide with its tangent force exactly balancing the system weight. Hence the value of C_T is C_{T_0}, as defined in Eq. (6). Unfortunately, as we shall see, the glide point, while statically stable, may be dynamically unstable, so that a given parachute may be unable to continue gliding, and instead may oscillate or perform a coning motion.

To investigate linearized stability of the glide point, we assume small disturbances from a steady glide in the x-z plane. Then the reference state is

$$\alpha = \alpha_0 \qquad C_T = C_{T_0} \qquad C_N = 0$$
$$u_0 = \sin\alpha_0 \qquad v = 0 \qquad w_0 = \cos\alpha_0 \tag{10}$$
$$p = q = \theta = \phi = 0$$

Now, define disturbance variables denoted by primes,

$$u' = u - u_0 \qquad v' = v \qquad w' = w - w_0$$
$$p' = p \qquad q' = q \qquad \theta' = \theta \qquad \phi' = \phi \tag{11}$$

Further, assume that the force coefficients are approximated by straight lines in the neighborhood of the glide point, as shown by the dotted lines in Fig. 2,

$$\alpha' = \alpha - \alpha_0 \qquad C_N = C_{N\alpha}\alpha' \qquad C_T = C_{T_0} + C_{T\alpha}\alpha' \tag{12}$$

If we substitute Eqs. (11) and (12) into Eqs. (5) and neglect squares and higher powers of disturbance variables, we arrive at the following linearized equations of motion about the glide point:

$$\left[D + C_{N\alpha}\frac{\cos\alpha_0}{(2k)}\right]u' - \left[C_{N\alpha}\frac{\sin\alpha_0}{(2k)}\right]w' +$$
$$\left[\cos\alpha_0\left(1 - \frac{C_{N\alpha}}{2k(1+r_c)}\right)D + \frac{C_{T_0}}{(2k)}\right]\theta' = 0 \tag{13}$$

$$\frac{1}{2k}(C_{T\alpha}\cos\alpha_0 + 2C_{T_0}\sin\alpha_0)u' +$$
$$\left[D + \frac{1}{2k}(2C_{T_0}\cos\alpha_0 - C_{T\alpha}\sin\alpha_0)\right]w' +$$
$$\left[\sin\alpha_0 - \frac{C_{T\alpha}\cos\alpha_0 + 2C_{T_0}\sin\alpha_0}{2k(1+r_c)}D\right]\theta' = 0 \tag{14}$$

$$-\frac{C_{N\alpha}\cos\alpha_0}{2i(1+r_c)}u' + \frac{C_{N\alpha}\sin\alpha_0}{2i(1+r_c)}w' +$$
$$\left[D^2 + \frac{C_{N\alpha}\cos\alpha_0}{2i(1+r_c)^2}D + \frac{C_{T0}r_{ch}}{2i(1+r_c)}\right]\theta' = 0 \tag{15}$$

$$Dv' - [\cos\alpha_0 D + C_{T_0}/(2k)]\phi' = 0 \tag{16}$$

$$[D^2 + C_{T_0}r_{ch}/2i(1+r_c)]\phi' = 0 \tag{17}$$

where the symbol D is the operator d/dt^*. For a detailed derivation of these five equations, see Wolf.[15]

These linearized relations have the valuable property that the longitudinal and lateral motions are uncoupled. That is, Eqs. (13–15) describe the longitudinal or pitching motion in the glide plane and contain only the in-plane variables (u', w', θ'), whereas Eqs. (16) and (17) describe the lateral motion normal to the glide plane. Thus the longitudinal and lateral stability of a symmetric parachute may be studied separately, similar to the study of aircraft linearized stability.[14]

Longitudinal Stability

Since Eqs. (13–15) are linear with constant coefficients, the solutions must be of the exponential form $e^{\lambda t^*}$, where λ is a constant. Setting u', w', and θ' in this exponential form and substituting, we obtain, by requiring the determinant of the coefficients to be zero, a fourth-order algebraic equation for the constant λ,

$$\lambda^4 + C_1\lambda^3 + C_2\lambda^2 + C_3\lambda + C_4 = 0 \tag{18}$$

where each of the constants C_i are linear functions of $C_{N\alpha}$

$$C_1 = E_1C_{N\alpha} + E_2 \qquad C_2 = E_3C_{N\alpha} + E_4$$
$$C_3 = E_5C_{N\alpha} + E_6 \qquad C_4 = E_7C_{N\alpha} \tag{19}$$

and, finally, the constants E_i are given as follows:

$$E_1 = \cos\alpha_0[k + i(1+r_c)^2]/2ki(1+r_c)^2$$
$$E_2 = (2C_{T_0}\cos\alpha_0 - C_{T\alpha}\sin\alpha_0)/2k$$
$$E_3 = C_{T_0}[k + i(1+r_c)^2 + k^2(1+r_c)]/2k^2i(1+r_c)^2$$
$$E_4 = C_{T_0}r_{ch}/2i(1+r_c) \tag{20}$$
$$E_5 = C_{T_0}\cos\alpha_0(3 + r_{ch})/4ki(1+r_c)$$
$$E_6 = C_{T_0}r_{ch}(2C_{T_0}\cos\alpha_0 - C_{T\alpha}\sin\alpha_0)/4ki(1+r_c)$$
$$E_7 = C_{T_0}{}^2(1+r_{ch})/4k^2i(1+r_c)$$

For any given system parameters, the constants C_i may be calculated and Eq. (18) solved for the four roots. For stability, it is necessary that C_4 be positive (static stability), which is true if $C_{N\alpha}$ is positive, since E_7 is always positive. This confirms the earlier discussion of stable gliding.

For dynamic stability, the real parts of the four roots must all be negative, which is ensured[14] if

$$C_1, C_2, C_3, \text{ and } C_4 > 0 \tag{21}$$

and if

$$C_3(C_1C_2 - C_3) - C_1{}^2C_4 > 0 \tag{22}$$

Equation (21) is also satisfied if $C_{N\alpha}$ is positive, a condition already required.

Equation (22) leads to a quadratic equation in $C_{N\alpha}$

$$K_1 C_{N\alpha}^2 + K_2 C_{N\alpha} + K_3 > 0 \tag{23}$$

where the constants K_i are

$$K_1 = E_1(E_3E_5 - E_1E_7)$$

$$K_2 = E_5(E_2E_3 - E_1E_4 - E_5) + E_1(E_3E_6 - 2E_2E_7)$$

$$K_3 = E_2(E_4E_5 + E_3E_6 - E_2E_7) + E_6(E_1E_4 - 2E_5)$$

Equation (23) yields the minimum value $C_{N\alpha}$ (min) required for dynamic stability,

$$C_{N\alpha}(\min) = -K_2/2K_1 + (K_2^2/4K_1^2 - K_3/K_1)^{1/2} \tag{24}$$

It will be seen that Eq. (24) is fairly restrictive and difficult for most parachute shapes to meet.

Numerical Stability Results

Equation (24) may be used to make parametric studies of longitudinal stability. However, the parameters k, i, r_c, and r_{ch} are not very significant physically, because the hydrodynamic inertia is mixed into all of them. Perhaps a more logical group would be the following four:

V_0^2/gL = the descent Froude number

D_0/L = the chute slenderness ratio

m_c/m_p = the canopy-to-load mass ratio

C_{T_0} = the gliding force coefficient

where D_0 is the nominal diameter of the canopy.

The dimensionless hydrodynamic mass B_m, defined as

$$B_m = 6m_{ch}/\pi\rho D_0^3 \tag{25}$$

relating m_{ch} to a sphere of air of diameter D_0, has been measured[16] and shown to vary considerably with porosity. The hydrodynamic moment of inertia factor

$$B_i = 60I_{ch}/\pi\rho D_0^5 \tag{26}$$

has also been measured[17] as a function of porosity. To be exact, both B_m and B_i are tensors with significant directional variation. However, from assumption 4, we shall approximate them here as average scalar values.

Experimental values of B_m (Ref. 16) are approximately 0.7 at zero porosity, dropping sharply to approximately 0.03 at 40% geometric porosity. Similarly, B_i is approximately 0.23 at zero porosity,[17] dropping to 0.04 at 40% porosity.

The four new practical parameters are related to those of Eqs. (6) as follows:

$$\left.\begin{aligned} k &= \tfrac{1}{2}C_{T0}V_0^2/(gL) + \tfrac{2}{3}B_mD_0/L \\ r_{ch} &= \frac{2B_mD_0/L}{3k - 2B_mD_0/L} \\ r_c &= (m_c/m_p)(1 + r_{ch}) + r_{ch} \\ i &= kr_c/(1 + r_c)^2 + B_i(D_0/L)^3/15 \end{aligned}\right\} \tag{27}$$

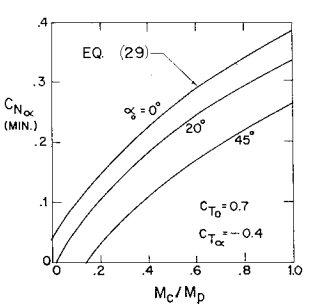

Fig. 3 Effect of glide angle on parachute stability ($V_0^2/gL = D_0/L = 1.0$, zero porosity)

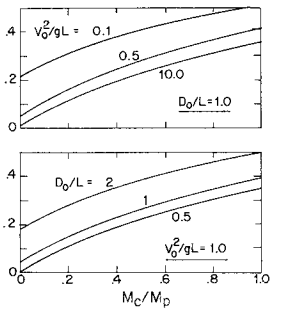

Fig. 4 Effect of Froude number and slenderness ratio on stability (C_{T_0} = 0.7, zero porosity).

For comparison with the stability criterion, Eq. (24), experimental values of $C_{N\alpha}$ and $C_{T\alpha}$ are needed. Reference 2 gives wind-tunnel results for ten different canopy shapes with varying effective porosity. For all ten shapes, the measured values of $C_{T\alpha}$ lie between 0.0 and −0.4, while the values of $C_{N\alpha}$ lie between 0.0 and +0.4. The maximum effect of $C_{T\alpha}$ on glide stability can thus be shown by evaluating Eq. (24) for $C_{T\alpha} = -0.4$. A typical result is shown in Fig. 3 for various glide angles of a nonporous canopy. It is seen that a negative $C_{T\alpha}$ has a stabilizing effect at finite glide angles. If $C_{T\alpha}$ is set equal to 0.0, the curves collapse to the single curve marked $\alpha_0 = 0°$, which is the conservative or maximum value of $C_{N\alpha}$(min). Figure 3 also shows that a heavily loaded parachute (small m_c/m_p) is more stable than a lightly loaded system.

Conservative Glide-Stability Criterion

A conservative and greatly simplified expression results if one sets $C_{T\alpha} = 0$ in Eqs. (13–15). The determinant of coefficients reduces to a cubic,

$$\lambda^3 + C_1\lambda^2 + C_2\lambda + C_3 = 0 \tag{28}$$

where

$$C_1 = \tfrac{1}{2}C_{N\alpha}(1/k + 1/i(1 + r_c)^2)$$

$$C_2 = (C_{N\alpha} + C_{T_0}r_{ch})/2i(1 + r_c)$$

$$C_3 = C_{N\alpha}C_{T_0}(1 + r_{ch})/4ki(1 + r_c)$$

which is independent of the angle α_0. The Routh stability criterion for a cubic is $C_1C_2 = C_3$, which results in a very simple expression for $C_{N\alpha}$(min)

$$C_{N\alpha}(\min) = C_{T_0}\{[i(1 + r_c)^2 - kr_{ch})/[i(1 + r_c)^2 + k]\} \tag{29}$$

Equation (29) is very similar to a criterion for stable vertical descent given by Heinrich and Rust.[8]

Using Eq. (29) for a conservative estimate, the general effects of Froude number and slenderness ratio are shown in Fig. 4. It is seen that increased stability is achieved by a more rapid descent (large V_0^2/gL) and by long lines (small D_0/L). Note that the two effects are opposing if one merely changes L.

Figure 5 illustrates the effect of C_{T_0} and porosity, showing that the high-drag body is less stable. The effect of porosity is a slight increase in stability through a decrease in the hydrodynamic inertia terms. A more important effect of porosity is the fact that the force coefficients themselves

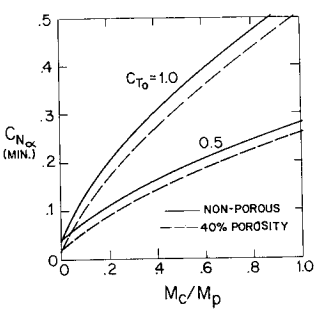

Fig. 5 Effect of tangent force and porosity on stability ($V_0^2/gL = D_0/L = 1.0$).

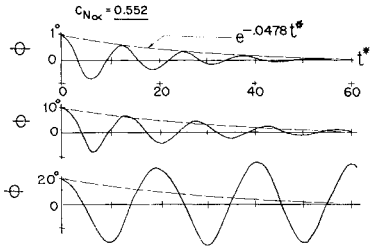

Fig. 6 Computer solutions for 1°, 10°, and 20° pitch displacements of the stable system.

change greatly with porosity,[2] which is not accounted for in Fig. 5.

From the data of Ref. 2, we find that most parachutes simply cannot develop sufficient $C_{N\alpha}$ to be glide stable except at high load masses, high descent speeds, and low effective porosity. For example, the personnel guide surface canopy, which has low $C_{N\alpha}$ and high (m_c/m_p), would be expected to oscillate rather than glide. This is evident from the computer solutions of Ludwig and Heins[12] for personnel parachutes.

Lateral Dynamic Stability

The lateral motion, Eqs. (16) and (17), is clearly much simpler and easily yields the following stability polynomial:

$$\lambda[\lambda^2 + C_{T_0} r_{ch}/2i(1 + r_c)] = 0 \tag{30}$$

The real part of all three roots is obviously zero. Hence, lateral small disturbances will lead to neutrally stable oscillations, although Eq. (24) must also be satisfied to keep all disturbances small. Thus a coning motion of an otherwise stable system cannot ensue from a small lateral disturbance, but instead is strictly a large-disturbance phenomenon.

Large-Disturbance Studies

To indicate the limitations of the previous linearized analysis, some exact computer solutions of Eqs. (5) will be shown. To this end, we select a simple but fairly realistic parachute as our basic system.

$$C_{T_0} = 0.7 \qquad C_{T\alpha} = -0.1 \qquad \alpha_0 = 25°$$
$$k = i = 1.0 \qquad r_c = r_{ch} = 0.1 \tag{31}$$

We will vary $C_{N\alpha}$ to show different effects. Both Eqs. (24) and (29) predict that $C_{N\alpha}(\min) = 0.352$. We select for study two systems on either side of this value: 1) stable, $C_{N\alpha} = 0.552$; and 2) unstable, $C_{N\alpha} = 0.152$. Simple polynomial expressions will be used for the variation of the force coefficients with angle of attack,

$$C_N(\alpha) = \alpha_0 C_{N\alpha}(\alpha/\alpha_0)(\alpha/\alpha_0 - 1)$$
$$C_T(\alpha) = C_{T_0} + \tfrac{1}{2} C_{T\alpha}\alpha_0(\alpha^2/\alpha_0^2 - 1) \tag{32}$$

which closely resemble the curves in Fig. 2.

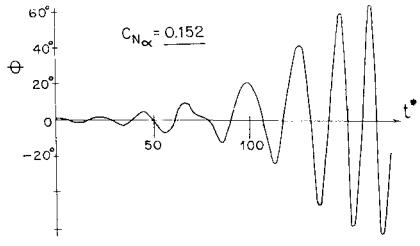

Fig. 7 Response of the unstable system to a 1° pitch displacement.

Longitudinal Disturbances

We first test the apparently stable system with various-sized longitudinal disturbances: $\theta' = 1°$, 10°, and 20°. The complete linear theory, Eq. (18), predicts an exponential damping rate of $e^{-.0478t^*}$, with a dominant short period of $T^* = 13.03$ (the long period mode damps out rapidly). For comparison, the simpler theory, Eq. (28), gives a damping rate $e^{-.0518t^*}$ and a period $T^* = 12.87$, reasonably accurate considering the reduction in computation.

Figure 6 shows the response $\theta(t^*)$ from the computer solution for each of the three disturbances. The 1° response is in nearly perfect agreement with the linear theory. The 10° disturbance still damps out, but at a lesser rate than the linear prediction. In contrast, the 20° case does not damp but instead jumps to a large angle (±32°) oscillation which persists. The angle of attack also oscillates between ±32°, which is outside the limits $\pm\alpha_0$. The explanation is that the 20° disturbance is sufficient to throw the parachute over the lower hump of the C_N curve and across to the negative α side. In rare cases, the chute will again damp to a stable glide at $(-\alpha_0)$, but usually the final condition is a pitching oscillation at some angle greater than α_0. A rule of thumb is that a parachute which is stable in the linearized sense will jump to a large angle pitching oscillation if struck with a disturbance greater than one-half its stable angle α_0.

To test the unstable system, we need only try the single disturbance $\theta' = 1°$ and let the system do the rest. The response is given in Fig. 7, showing that the motion diverges to a very large amplitude oscillation of ±65°. Other size disturbances would approach the same final pitching motion, which is characteristic of the unstable system in longitudinal motion.

Lateral Disturbances

The lateral behavior of the stable system can be observed by comparing two disturbances, $\phi' = 1°$ and 40°. The resulting responses are shown in Fig. 8. The motion for $\phi' = 1°$ is a neutral sinusoid, in agreement with the linear theory. The period $T^* = 35.2$ can be predicted from Eq. (30). The induced longitudinal motion θ is a negligibly small fraction of a degree, too small to show in the figure.

In contrast, the large disturbance of 40° immediately induces a longitudinal motion $\theta(t^*)$ of comparable magnitude. Both θ and ϕ approach a stable oscillation (not a pure sinusoid) with equal amplitudes of 38.7°, with θ lagging ϕ. To visualize this motion, we note that the canopy is falling directly downward at a resultant velocity $V_c^* = 1.038$, while the load is moving downward along a helical path of constant radius. The parachute centerline maintains a constant angle with the vertical of 38.7° (identical to the amplitude of θ and ϕ) and the centerline rotates about the vertical with a constant angular rate of 0.493. In short, the 40° lateral disturbance has thrown the stable parachute into a uniform vertical coning motion.

The unstable system, when struck with a 1° lateral disturbance, also diverges into a coning motion, as shown in Fig. 9. The lateral motion induces very small glide-plane motions which build up exponentially because of the longitudinal instability. Since the induced motion is only $\theta' =$

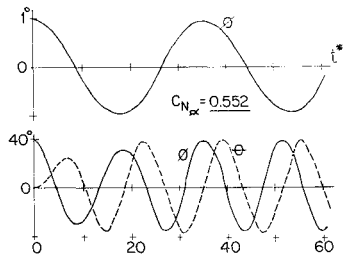

Fig. 8 Stable system response to 1° and 40° lateral displacements.

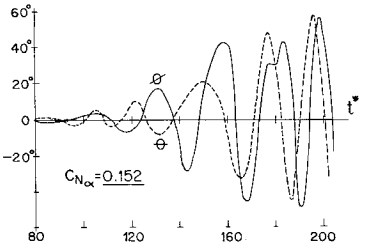

Fig. 9 Unstable system response to a 1° lateral displacement.

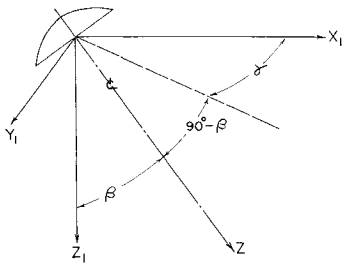

Fig. 10 Illustration of coning angles.

0.02°, the build-up time is long; hence, Fig. 9 is begun at $t^* = 80$. The final motion is again a pure vertical coning, this time at a larger angle $\beta = 58.6°$, where β is the coning angle illustrated in Fig. 10. Since the only difference in the two systems is the value of $C_{N\alpha}$, it is clear that $C_{N\alpha}$ has a large effect on the coning angle. Also, this time the angular coning rate $\dot{\gamma}$ is 0.606, where γ is the angle in the horizontal plane as illustrated by Fig. 10. The two angles, β and γ, are sufficient to describe a pure vertical coning attitude. In terms of the Euler angles θ, ϕ, and ψ, these two angles may be written as follows:

$$\cos\beta = \cos\theta \cos\phi$$
$$\cos\gamma = \csc\beta(\cos\phi \sin\theta \cos\psi + \sin\phi \sin\psi) \tag{33}$$

One may conclude that a linearized stable parachute is neutrally stable to a small lateral disturbance but may jump into a vertical coning motion if hit with a large lateral displacement. A linearized unstable parachute will be driven into a coning motion by any lateral displacement.

Coning Analysis

The computer solutions shown in Figs. 8 and 9 give the key to the mathematical form of the functions involved in vertical coning. From this key, a complete algebraic theory of coning can be constructed. The velocity w is constant, while u and v are sinusoidal with equal amplitude and 90° out of phase. The angular velocities p and q are also sinusoidal, of equal amplitude, 90° out of phase, and together lag u and v by constant phase angle σ. Hence the proper functions are

$$u = u_0 \cos(\omega t^*) \qquad v = u_0 \sin(\omega t^*)$$
$$w = V_c^* \cos\beta = \text{const} \tag{34}$$
$$p = p_0 \cos(\omega t^* + \sigma) \qquad q = p_0 \sin(\omega t^* + \sigma)$$

If we substitute Eqs. (34) into the equations of motion, Eqs. (5), using Eqs. (33) to eliminate θ and ϕ, we find that each equation of motion is satisfied identically, i.e., Eqs. (34) are the exact solution for coning. What remains are seven algebraic relations involving u_0, p_0, σ, β, ω, $\dot{\gamma}$, and V_c.

After considering manipulation, we are left with a single transcendental equation for finding the coning angle β

$$C_T/C_N = a \tan\beta + b \cot\beta$$

where

$$b = [(1 + r_c)^2 + 1]/[(1 + r_c)^2 - r_{ch}] \tag{35}$$

and

$$a = [1 + r_{ch}bk/i]/(1 + r_c)^2$$

and where the coefficients C_T and C_N are evaluated at the angle of attack $\alpha = \beta$. The quantities a and b are system constants and do not involve β. For our sample parachute, Eq. (31), $a = 0.99$ and $b = 1.99$. The ratio C_T/C_N depends upon the choice of $C_{N\alpha}$, whether 0.552 or 0.152, and the polynomial curve fits, Eqs. (32). Since the right-hand side of Eq. (35) is always positive, the coning angle must be in a region of positive C_N, which means that β must be greater than α_0.

Table 1 SAND system parameters

Altitude, ft	k	i	r_c	r_{ch}
180,600	198.0	11.0	0.051	0.0006
143,300	49.8	2.76	0.052	0.0023
121,800	20.0	1.11	0.057	0.0066

Figure 11 shows a graphical solution for the coning angle for each of the two cases of $C_{N\alpha}$, 0.552 or 0.152. The solutions are seen to be 38.7° and 58.6°, respectively, in perfect agreement with the computer solutions for coning.

Once β is known, the rate of fall of the canopy can be calculated from the relation

$$V_c^{*2} = C_{T_0} \sin\beta/(bC_N) \tag{36}$$

and the angular rate of coning $\dot{\gamma}$ can be calculated from the expression

$$\dot{\gamma}^2 = [(1 + r_c)/2k](C_T V_c^{*2} - C_{T_0} \cos\beta) \csc^2\beta \tag{37}$$

Equations (35–37) give the most important coning variables. Other supplementary relations are

$$\omega = \dot{\gamma} \cos\beta$$
$$\dot{\gamma} = -(1 + r_c)V_c^* \tan(\sigma) \tag{38}$$

As in the stability analysis, these coning relations could be studied for parametric effects, using say, the practical parameters from Eqs. (27). It is necessary also to assume some force coefficient curves, say, Eqs. (32), since the coning does not occur at the glide point. One finds that a single coning solution exists for any given system, and that the only two parameters which have any great effect on coning are α_0 and $C_{N\alpha}$. There is little point in making charts of coning solutions because, unlike the glide point study, no exact criterion for coning motion to ensue can be established. One might think that the larger coning angles might be more difficult to achieve, but we have seen in Fig. 11 that large β probably implies glide-point instability, and hence, is very susceptible to coning. The glide-stable systems also cone easily if struck with the proper sized lateral displacement. The authors can only conclude that the coning motion as outlined here is always a possibility if the disturbance conditions warrant. However, it is possible that, at these large angles of attack, some unaccounted-for pitching moment variations may develop such as an unusual variation in the canopy center of pressure, thus precluding a stable coning motion. To the authors' knowledge, such center-of-pressure

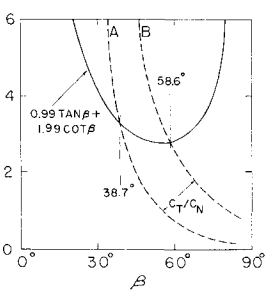

Fig. 11 Graphical coning angle solution for the two illustrative cases. (A: $C_{N\alpha}$ = 0.552; B: $C_{N\alpha}$ = 0.152).

Table 2 Coning calculations for SAND

Altitude, ft	β	$\dot{\gamma}$	Theoretical coning rate, rps	Observed rate, rps
180,600	39.3°	0.0352	0.105	0.10
143,300	39.0°	0.0702	0.110	0.12
121,800	38.5°	0.114	0.115	0.22

variations have not been measured, hence, the use of our somewhat dubious assumption 6. It is also interesting to note that this coning analysis is not limited to parachutes but is mathematically valid for any free-falling body of revolution. Such a body may cone if it can develop aerodynamic forces which satisfy Eq. (35).

Comparison with Coning Data

A coning motion was observed during a test flight of the Sandia Corporation's SAND sampler vehicle.[18] This system employs a 14.3% full extended skirt parachute of 50.5-ft nominal diam to lower a 700 lb payload from altitudes of several hundred kilofeet. For the test flight, the dimensionless parameters at three different altitudes are presented in Table 1. Note that the hydrodynamic parameter r_{ch} is very small because of the high altitude. The force coefficients are not known at these altitudes, but another analysis[19] assumed the canopy to have an effective porosity of 0.042, for which Ref. 2 gives $C_{T_0} \doteq 0.8$, $\alpha_0 \doteq 19°$, and $C_{N\alpha} \doteq 0.2$. Using Eq. (29) and Table 1, we calculate $C_{N\alpha}(\min) = 0.045$ for all three altitudes; hence, the system is glide-stable. In spite of this, the system coned continuously at an angle $\beta \doteq 40°$ throughout the altitude range.

Numerical calculation of Eqs. (35) and (37) for the parameters in Table 1 is given in Table 2. The agreement is good except for the coning rate at the lowest altitude. However, the lack of knowledge of the canopy effective porosity could easily account for this discrepancy.

Conclusions

It has been shown that a simplified five-degree-of-freedom analysis can yield considerable information about parachute dynamic stability. Subject to the simplifying assumptions listed in the beginning, the conclusions of this study are:

1) A system that is glide-stable from Eq. (24) will damp out small longitudinal glide-point disturbances and be neutrally stable for small lateral fluctuations.

2) A system that is glide-unstable will diverge to a large angle pitching oscillation if disturbed longitudinally and to a large angle vertical coning motion if disturbed laterally.

3) A stable parachute with finite α_0 will jump into a pitching oscillation if hit with a large longitudinal disturbance, and will jump into vertical coning if given a large lateral displacement. Exact algebraic expressions are given for the coning motion, which is apparently a stable mode of descent.

The validity of these conclusions should be established or disproven by experiment. There is a need not only to test the given stability criteria but also to examine the basic assumptions critically.

References

[1] *U.S. Air Force Parachute Handbook*, Wright Air Development Center, TR 55-265 (December 1965).

[2] Heinrich, H. G. and Haak, E. L., "Stability and drag of parachutes with varying effective porosity," Wright-Patterson Air Force Base, ASD-TDR-62-100 (September 1962).

[3] Heinrich, H. G., "Experimental parameters in parachute opening shock theory," Dept. of Defense, Shock & Vibration Bulletin 19, (February 1953).

[4] Meyer, E. J., "Results of a dynamic stability test using weight-scaled SAND parachute systems," Sandia Corp., Albuquerque, N.Mex., Rept. SC-4771(RR) (March 1963).

[5] Henn, H., "Descent characteristics of parachutes," Royal Aeronautical Establishment Translation of German Rept. ZWB/UN/6202 (October 1944).

[6] Brown, W. D., *Parachutes* (Pitman and Sons Ltd., London, 1951).

[7] Lester, W. G. S., "A note on the the theory of parachute stability," Royal Aeronautical Establishment, Farnborough, TN Mechanical Engineering 358 (July 1962).

[8] Heinrich, H. G. and Rust, L. W., "Dynamic stability of a parachute point-mass load system," Wright-Patterson Air Force Base, FDL-TDR-64-126 (June 1965).

[9] Heinrich, H. G., "Drag and stability of parachutes," Aeronaut. Eng. Rev., **15** 73–81 (June 1956).

[10] Ludwig, R., "Stabilitatsuntersuchungen an Fallschirmen mit Hilfe eines Digital und Analogrechners," Vorabdruck des Techniques de Calcul Analogique et Numerique en Aeronautique, Liege, Belgium (September 1963).

[11] Ludwig, R. and Heins, W., "Investigations on the dynamic stability of personnel guide surface parachutes," AGARD Flight Mechanics Panel Meeting, Turin, Italy (April 1963).

[12] Ludwig, R. and Heins, W., "Theoretical studies of the dynamic stability of parachutes," Jahrb. 1962 Wiss. Ges. Luft Raumfahrt, Faraday Transl. (November 1964).

[13] Stimmler, F. J. and Ross, R. S., "Drop tests of 16,000 sq. in. model parachutes," U.S. Air Force TR 5867 (1954).

[14] Etkin, B., *Dynamics of Flight* (John Wiley & Sons Inc., New York, 1959).

[15] Wolf, D. F., "An investigation of parachute dynamic stability," M.S. thesis, Univ. of Rhode Island (1965).

[16] Ibrahim, S. K., "Apparent added mass and moment of inertia of cup-shaped bodies in unsteady incompressible flow," Ph.D. thesis, Univ. of Minnesota (1965).

[17] Ibrahim, S. K., "Experimental determination of the apparent moment of inertia of parachutes," Wright-Patterson Air Force Base, FDL-TDR-64-153 (April 1965).

[18] Melvin, J. W., "Data reduction report (trajectory), Sandia test RY-12," Sandia Corp., Albuquerque, N.Mex. (March 1963).

[19] Vaughn, H. R. and Matejka, D. Q., "Dynamic analysis of the SAND sampler," Sandia Corp., Albuquerque, N.M., Project SAND Final Program Reprt., SC-RR-65-286, Vol. III (September 1965).

[20] White, F. M. and Wolf, D. F., "The dynamic stability of a freely descending parachute," Sandia Corp. Albuquerque, N.Mex., SC-TM-66-2 (1966).